Vacuum 141 (2017) 15–21

Contents lists available at ScienceDirect

Vacuum

journal homepage: www.elsevier.com/locate/vacuum

Photoluminescence and enhanced chemical reactivity of amorphous SiO_2 films irradiated with high fluencies of 133-MeV Xe ions

L. Vlasukova [a, *], F. Komarov [b], I. Parkhomenko [a], V. Yuvchenko [b], O. Milchanin [b], A. Mudryi [c], V. Zyvul'ko [c], A. Dauletbekova [d], A. Alzhanova [d], A. Akilbekov [d]

[a] Belarusian State University, Nezavisimosty Ave. 4, 220030, Minsk, Belarus
[b] A. N. Sevchenko Institute of Applied Physics Problems, Kurchatov Str. 7, 220045, Minsk, Belarus
[c] Scientific and Practical Materials Research Center, National Academy of Sciences of Belarus, P. Brovki Str. 17, 220072, Minsk, Belarus
[d] L.N. Gumilyov Eurasian National University, Munaitpasova Str. 5, Astana, Kazakhstan

ARTICLE INFO

Article history:
Received 4 November 2016
Received in revised form
3 March 2017
Accepted 4 March 2017
Available online 6 March 2017

Keywords:
SiO_2/Si
Swift heavy ions
High fluencies
Photoluminescence
Chemical etching
Thermal annealing

ABSTRACT

SiO_2/Si structures have been irradiated with 133 MeV Xe^{+17} ions at fluencies of (10^{10}–5×10^{14}) cm^{-2}. The structure transformation and light-emitting properties of irradiated SiO_2 films were studied using RS, SEM, TEM and PL techniques as well as chemical etching in 4% solution of hydrofluoric acid (HF). An intensive photoluminescence in visible range was registered from the samples irradiated at a fluence of 10^{14} cm^{-2} and higher. Simultaneously, it was found a drastic increase of SiO_2 etch velocity in HF solution for the irradiated samples. Annealing (1100 °C, 2 h) of irradiated samples resulted in PL quenching and etch velocity recovery practically to the value of non-irradiated SiO_2. It was concluded that radiative oxygen deficient centers are responsible for the PL appearance. It was also shown that the etch velocity ratio of the irradiated and virgin SiO_2 in 4%-HF (V_{irr}/V_{virgin}) can be used in order to estimate the radiation damage in SiO_2 matrix irradiated with high fluencies of swift heavy ions.

1. Introduction

Swift heavy ion (SHI) projectiles can produce point defects, defect clusters and ion latent tracks – extended damage regions along ion trajectories - in an irradiated target. Ion tracks were first observed in nuclear fission reactors [1] and since then they have been widely studied due to their growing list of technological applications. It is possible to modify thin films of insulators by means of SHI irradiation. Thin SiO_2 films integrated into silicon wafers are of special interest for nanotechnology. The passage of swift ions through SiO_2 and some other insulators is usually described by the thermal spike model [2–5]. In this model, it is assumed that latent tracks are the result of interaction of the projectile ions with the target electrons, and an initial track size is determined by a cylindrical molten zone (future latent track) created along the ion trajectory. Owing to a different chemical reactivity than virgin matrix, the latent track regions in SiO_2 can be transformed into nano- or microchannels by means of etching in hydrofluoric acid (HF) solutions [6–9]. The other promising field is a possibility for controlling the shape and size of nanoclusters embedded in dielectric matrix via SHI irradiation. The authors of Refs [10–13] have reported a shape transformation of Ag, Au, Co and InAs nanoparticles embedded into amorphous SiO_2 films from spherical one to conical or elongated along the SHI beam direction. A new wave of interest in studying the SHI–SiO_2 interaction is due to a possible usage of SHIs for the creation of Si-based light-emitting nanostructures via SiO_2 disproportionation in the ion tracks [14,15].

Moreover, when solar cells and MOS structures with insulating silica layers are in outer space equipment, the radiation defects generation in SiO_2 is possible. The point defects and defect clusters play a very important role in the silica's electronic properties and could modify the electronic device's characteristics. Thus, radiation induced defects in silica deserve a special attention in the modern electronic technology, too.

Latent track regions in SiO_2 are referred to as radiation damaged areas. In etching solution, the damaged areas of irradiated sample are etched much faster than the undamaged ones [16]. It provides an opportunity to transform the tracks into pores by means of

* Corresponding author. Belarusian State University, Kurchatova Str. 5, 220045 Minsk, Belarus.
E-mail address: vlasukova@bsu.by (L. Vlasukova).

http://dx.doi.org/10.1016/j.vacuum.2017.03.007
0042-207X/

controlled chemical etching. Though, this possibility could be realized only for low SHIs fluencies. Multiple tracks overlapping takes place at high fluencies, and the *a*-SiO_2 layer, on the whole, becomes damaged. Hence, the etch velocity of irradiated SiO_2 matrix (V_{irr}) in HF solution should be higher in comparison with the etch velocity of virgin one (V_{virgin}). In our study, we have used this parameter (V_{irr}) to estimate the SHI-induced damage in SiO_2 matrix.

The aim of this paper is to investigate chemical reactivity and light-emitting properties of SiO_2 layers irradiated with high SHIs fluencies. We have also tried to elucidate a correlation between SHI-induced photoluminescence (PL) and structural transformations of SiO_2 as well as to estimate the influence of high-temperature treatment on the etch velocity and the photoluminescence of irradiated SiO_2 layers.

2. Methods

The 1×1 cm^2 samples were cut from the thermally oxidized Si (100) wafer. The thickness of SiO_2 film was ≈ 1 μm according to the ellipsometry data. These samples were afterwards irradiated with 133 MeV Xe^{17+} ions to fluencies ranging from 1×10^{10} to 5×10^{14} cm^{-2} at room temperature and at the normal incidence. Irradiation was conducted at the DC-60 cyclotron (Astana, Kazakhstan). After irradiation, a part of the samples was additionally annealed at 1100 °C for 2 h in Ar atmosphere.

The electronic energy loss S_e and the nuclear energy loss S_n for SiO_2/Si structure were simulated using the SRIM'2013 code [17]. We have calculated the diameter and lifetime of molten regions along the Xe ion trajectories in SiO_2 in the frame of inelastic thermal spike model [5]. It enables us to estimate a latent track size as well as to calculate an extent of latent track overlapping for our experimental conditions. The SiO_2 density was taken to be 2.2 g/cm^3 in computer simulations [18].

The surface morphology and microstructure were analyzed by scanning electron microscopy (SEM) and transmission electron microscopy in "cross-section" technique (XTEM). The scanning microscopy study was performed using a Hitachi S-4800 microscope at an electron-beam orientation perpendicular to the surface. The microstructure of irradiated SiO_2/Si samples was investigated by a 200-keV Hitachi H-800 microscope. The standard procedure of sample's mechanical polishing and thinning by ion milling was used in TEM cross-sections preparation. Raman scattering (RS) and photoluminescence (PL) were used to study optical properties of the samples. Raman spectra were measured using the micro-Raman setup Ntegra Spectra with a laser beam at $\lambda = 473$ nm. PL signal was excited by a He–Cd laser source at $\lambda = 325$ nm. All optical measurements were performed at room temperature.

The virgin and irradiated samples as well as the irradiated samples after annealing were treated in a 4% aqueous solution of hydrofluoric acid (HF) at room temperature for 6 min. A half of the surface of each sample was covered with wax prior etching. In order to avoid artefacts all the samples were etched in the same process (simultaneously). The thickness of SiO_2 layer for protected and unprotected regions of the etched samples was evaluated from laser ellipsometry ($\lambda = 632.8$ nm). Thus, we could estimate the thickness of SiO_2 layer removed during the HF-solution treatment. The etch velocity could be determined as a ratio of the removed layer thickness to the etching time.

3. Results and discussion

According to the SRIM code, S_e in the SiO_2 layer is nearly constant and amounts to ~13.5 keV/nm. This value is about 2 orders of magnitude higher than S_n in SiO_2. The calculated radius of molten region (future latent track) formed along the 133 MeV Xe ion trajectory in SiO_2 and its lifetime were 5.9 nm and 21.5 ps, respectively [5]. The molten region lifetime allows us speaking about the presence of the liquid phase in SiO_2 matrix and its subsequent solidification.

The question is if the calculated radius of molten region corresponds to the radius of resulting latent track. It is well known that direct observation of ion tracks in a-SiO_2 is a very difficult procedure due to a lack of sufficient contrast between the amorphous matrix and the track (see, for example [19]). That is why, a number of indirect methods such as IR absorption [16], small angle X-ray scattering (SAXS) [20] and track etching technique [21,22] were used successfully to quantify the sensitivity of amorphous SiO_2 under swift heavy ion irradiation. In the recent review [19], the results gathered by each of these techniques were compared with each other to gain a better understanding of track formation phenomena. The latent track radii deduced from IR spectroscopy, SAXS analyses as well as extrapolated ones from the etching experiments were plotted as a function of S_e for different specific beam energies ranged from 0.14 to 11 MeV/u. The S_e of Xe ions with 1 MeV/u in SiO_2 (our experimental conditions) is equal to ~ 13.5 keV/nm. According to the "radius versus S_e" dependence from Ref. [19] (obtained from SAXS data for Au ions at 0.14–0.94 MeV/u), the latent track radius amounts to ~ 5.5 nm at the 13.5 keV/nm. It is in a reasonable agreement with the calculated radius of molten region (5.9 nm). Hence, we can use the calculated value for preliminary estimation of the extent of latent track overlapping.

One can estimate the extent of latent track overlapping using the equation

$$K = \pi R_{tr}^2 \Phi,$$

where K denotes the extent of overlapping, R is the calculated radius of molten region and Φ is the ion fluence. The calculated K values are summarized in Table 1. One can see that track overlapping is negligible at the fluence of 1×10^{10} cm^{-2}. The irradiated area of silica is completely covered with tracks at the fluence of 1×10^{12} cm^{-2}. The further fluence increase results in multiple overlapping.

The surface morphology features of the samples under investigation were examined by SEM. Fig. 1 presents the SEM surface micrographs of the virgin SiO_2/Si and the samples irradiated to fluencies of 1×10^{12} cm^2 and 5×10^{14} cm^{-2} after etching in HF-solution. The surface of virgin SiO_2 layer is without any peculiarities (not shown), and etching does not result in any surface morphology changes (Fig. 1A). As it was mentioned above, a part of the surface of each sample was protected during the etch procedure and was not subjected to an influence of etch solution. Hence, the surface morphology of these regions is the same as for the as-irradiated SiO_2/Si samples before etching. Further, we will denote protected surfaces of the samples as the as-irradiated ones. Surprisingly, the pattern formation has been observed at the as-irradiated surfaces (Fig. 1C, E). Worm-like features have been evolved on the surface of the samples irradiated to the fluence of 1×10^{12} cm^{-2} (Fig. 1C). These features have got less pronounced (more coarse), and additional features of bright contrast (hillocks)

Table 1
The extent of track overlapping (K) for fluencies used in this experiment.

Fluence, cm^{-2}	K
1×10^{10}	~0
1×10^{12}	1
1×10^{14}	109
5×10^{14}	547

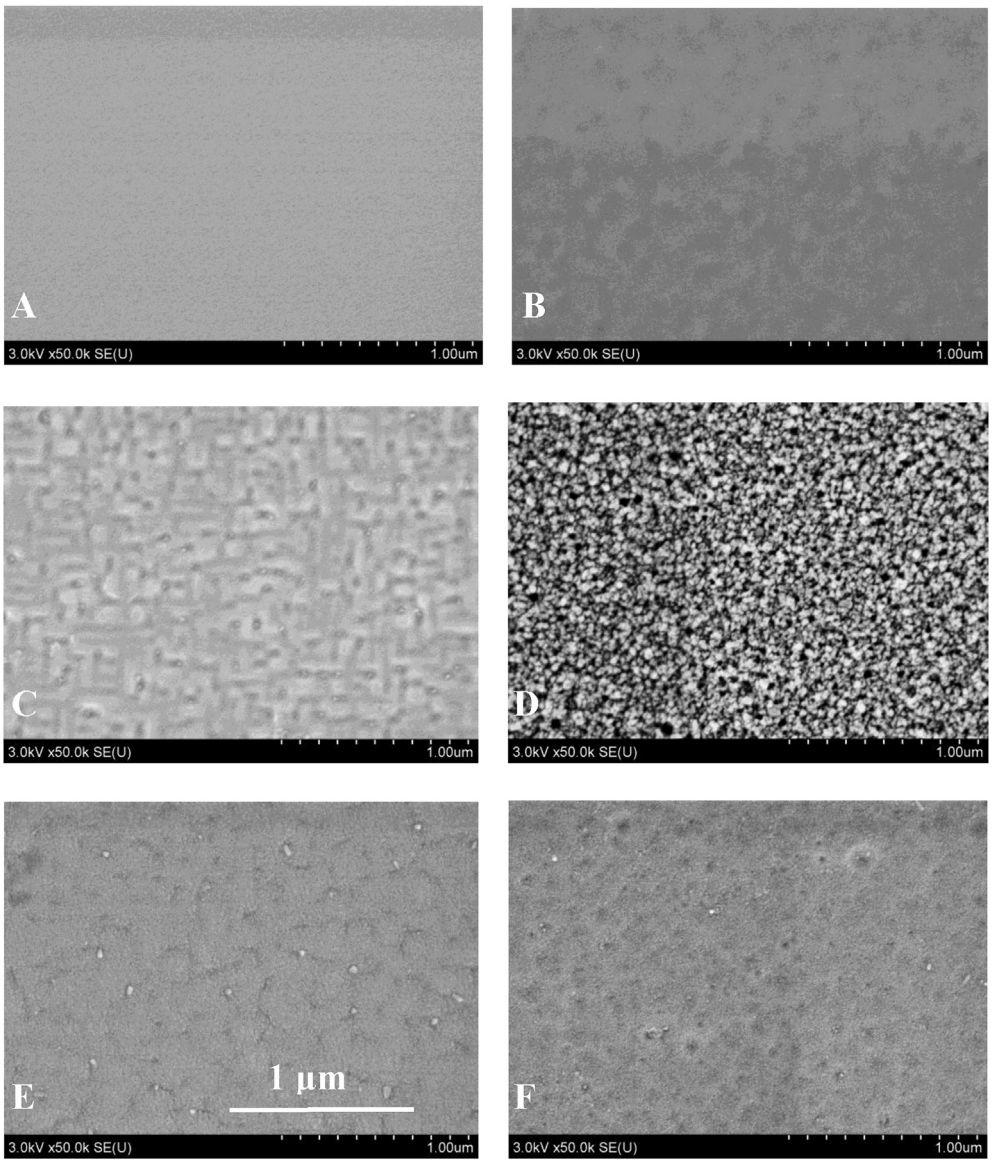

Fig. 1. The surface of SiO_2/Si samples after etching in 4% HF for 6 min: the virgin (without irradiation) sample (A), the sample irradiated with 133 MeV Xe^{17+} ions to the fluence of 5×10^{14} cm^{-2} and annealed at 1100 °C for 2 h (B), the sample irradiated with 133 MeV Xe^{17+} ions to the fluence of 1×10^{12} cm^{-2} (C, D) and the sample irradiated with 133 MeV Xe^{17+} ions to the fluence of 5×10^{14} cm^{-2} (E, F). The sample surface was protected during the etch procedure (C, E). The scale is the same for all micrographs.

have appeared with fluence increasing to 5×10^{14} cm^{-2} (Fig. 1E). A formation of self-organized surface patterns on a silica glass substrate due to high energy ion irradiation has been recently reported in Ref. [23]. As in our experiment, worm-like patterns on the surface of silica samples normally irradiated with 1.8 MeV Au^{2+} ions to the fluence higher than 5×10^{16} cm^{-2} were observed, too. The authors of Ref. [23] have explained the observed surface modification via compressive stresses generating in the near surface region during the irradiation. In our opinion, mechanisms of the pattern formation on the surface of ion-irradiated materials are complicated and not yet understood. A clearance of the origin of surface modification of irradiated samples is a subject of future investigations and beyond the scope of this paper.

After irradiation the samples were etched in 4% HF solution as described in Sect. 2. The etched surface of the sample irradiated to the fluence of 1×10^{12} cm^{-2} is characterized by overlapping irregular shape pores (Fig. 1D). Further fluence increasing results in a substantial surface transformation. Only a few shallow pits are observed on the etched surface of the samples irradiated to fluencies of 1×10^{14} (not shown) and 5×10^{14} cm^{-2} (Fig. 1F). The track overlapping values amount to 109 and 547 at 1×10^{14} and 5×10^{14} cm^{-2}, respectively (see Table 1). What is the reason for such inhomogeneous etching despite the complete damage overlapping at 10^{12} cm^{-2} and multiple one at higher fluencies? This effect can be explained by a complicated structure of individual tracks in a-SiO_2 demonstrated by Kluth et al. [20] recently using SAXS measurements. They revealed a track fine structure comprising a cylindrical core-shell configuration with a lower density core and a higher density shell as compared to unirradiated material. More recently, Kluth et al. [24] reported a steady state of nanoscale density fluctuations in a-SiO_2 irradiated with high fluencies of SHIs when the surface is completely covered by ion tracks. SAXS measurements and molecular dynamics simulations were consistent that these density fluctuations resulted from track overlapping where newly formed tracks annihilated (partially) pre-existing tracks. Apparently, well-developed

morphology (at 10^{12} cm^{-2}) and shallow pits (at higher fluencies), we have observed on the etched surfaces of irradiated samples are the signature of density fluctuations discussed in Ref. [24].

Fig. 1B depicts the view of the etched surface of the sample irradiated to the fluence of 5×10^{14} cm^{-2} and afterwards annealed at 1100 °C for 2 h. One can see substantial smoothening of the etched surface of the annealed sample. A similar effect (smoothening of the etched surface) has been observed for all irradiated and annealed samples (not shown). A disappearance of the as-irradiated surfaces patterns is observed after annealing, too. In consequence, the surface images of the etched and as-irradiated areas after annealing become the similar ones. This is not surprising as the thermal treatment leads to radiation damage recovery as it will be shown below from the etch velocity and PL data.

Fig. 2 presents the etch velocity in 4% HF solution for irradiated and annealed SiO_2 films as a function of ion fluence. V_{virgin} of non-irradiated sample amounts to 17.0 nm/min and is marked as a point at the vertical axis. The etch velocity of irradiated samples increases with the fluence and reaches the highest value (70.2 nm/min) at the fluence of 5×10^{14} cm^{-2}. One can see that the heat treatment at 1100 °C for 2 h results in the etch velocity recovery practically to its virgin value, obviously, due to damage annealing in the irradiated a-SiO_2.

For explanation of observed results, at first, let us discuss a mechanism of latent track transformation into a pore during chemical etching. A rearrangement of energetically favorable six-component rings consisting of SiO_4-tetrahedra into three- and four-component rings takes place along the latent SHI track in a-SiO_2 [16,25]. The increase of the number of small rings (with a decreased angle of the Si—O—Si bonds) leads to a decrease of the amorphous silicon dioxide volume [25,26]. This is a reason for the emergence of microscopic defects with stressed Si—O bonds in the form of paramagnetic E′ centers [27]. Oxygen deficient defects emerge at the damaged areas by means of the knock-on process of oxygen atoms [28]. The presence of E′ centers and oxygen deficient centers with strained bonds around them explains the higher etch velocity along the SHI track [27]. The difference of etch velocities between track region and undamaged SiO_2 matrix, in turn, results in the pore formation on the spot of latent track. Such scenario is realized for low SHI fluencies. Though, if the track density if high enough, at high fluencies, individual track regions are merged, and the SHI-induced microscopic defects with stressed Si—O bonds around them are distributed all over the SiO_2 matrix. We can suggest an enhanced etching rate of such material in comparison with virgin one. In our experiment, track overlapping begins at the fluence of 1×10^{12} cm^{-2} (see Table 1). Though, there is no substantial difference of the SiO_2 etch velocities between the samples irradiated to the fluence of 1×10^{10} or 1×10^{12} cm^{-2}. For comparison, the V_{irr}/V_{virgin} ratio amounts to 1.6 and 1.7 for fluencies of 1×10^{10} and to 1×10^{12} cm^{-2}, respectively. At 1×10^{14} cm^{-2}, multiple track overlapping takes place, and the number of microscopic defects increases substantially. The etch velocity of irradiated SiO_2 increases, too. At the fluence of 5×10^{14} cm^{-2} a further accommodation of defects responsible for enhanced etching rate results in the etch velocity drastic increasing. The V_{irr}/V_{virgin} ratio amounts to 2.2 and 4.1 for fluencies of 1×10^{14} cm^{-2} and 5×10^{14} cm^{-2}, respectively. Let us compare this ratio with the similar parameter V_T/V_B of the individual track etching process in a-SiO_2. In regarding to individual track etching, V_B is the etch velocity of the undamaged material, whereas V_T is the etch velocity of damaged material along the ion track. The V_T/V_B ratio is usually in the range of $2<V_T/V_B<4$ [9]. One can see that the V_{irr}/V_{virgin} ratio under multiple track overlapping conditions (obtained in our experiment) is in the same range. In other words, if the V_T/V_B ratio is a measure of track region damage at low SHI fluencies, then the V_{irr}/V_{virgin} ratio can be used in order to estimate the radiation damage in the SiO_2 matrix irradiated with high SHI fluencies.

Fig. 3 shows the PL and reflectance spectra for the virgin and irradiated samples. The PL spectrum of the virgin sample includes one low-intensive band centered at 450 nm. No additional features are found after the irradiation with the fluence of 1×10^{10} cm^{-2}. A new band centered at 550 nm appears in the spectrum of the sample irradiated with the fluence of 1×10^{12} cm^{-2}. Fluence increasing to 1×10^{14} cm^{-2} results in significant growth of PL intensity (by 10 times) and in appearance of the band set with maxima at 390 nm (ultra-violet), 450 nm (blue), 550 nm (green, the most intensive one) and 670 nm (red). The further fluence increase to 5×10^{14} cm^{-2} leads to the intensity redistribution between blue-violet and red bands and to a negligible red shift of green band in comparison with the sample irradiated at the fluence of 1×10^{14} cm^{-2}. We believe that these four PL bands cannot be

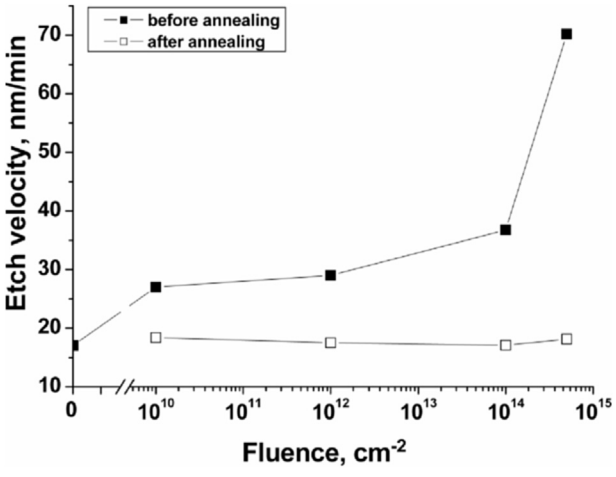

Fig. 2. The etch velocity of SiO_2 films irradiated at different fluencies: (-■-) as-irradiated samples, (–□–) irradiated samples after annealing at 1100 °C for 2 h (the lines are there to guide the eyes). The etch velocity of virgin sample is marked as a point at the vertical axis.

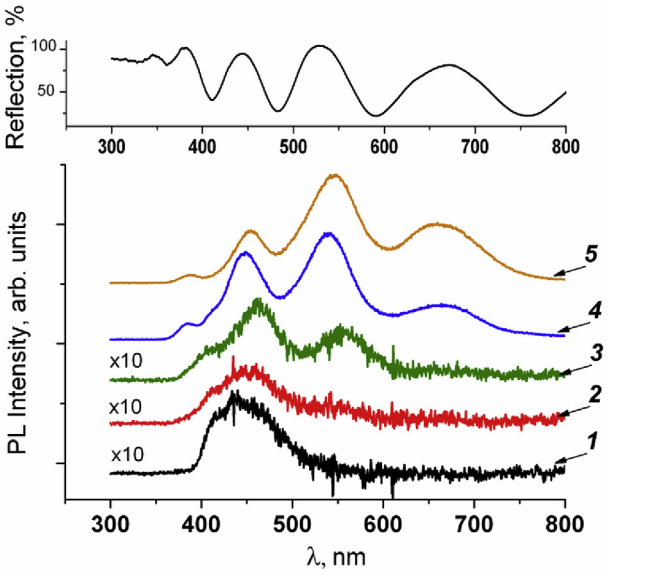

Fig. 3. PL spectra of SiO_2 films: virgin (1), after irradiation with 133 MeV Xe ions to the fluence of 1×10^{10} cm^2 (2), 1×10^{12} cm^2 (3), 1×10^{14} cm^2 (4) and 5×10^{14} cm^{-2} (5). The upper spectrum depicts the reflectance of the sample irradiated to the fluence of 1×10^{14} cm^{-2}.

attributed to different light-emitting sources. More likely, their appearance is caused by an interference effect. In this case, the thickness (d) of the film can be estimated from the PL spectra using the formula

$$d = \frac{\lambda_1 \lambda_2}{2n(\lambda_2 - \lambda_1)},$$

where n=1.46 is the average refractive index of the film in the spectral range under investigation, and λ_1 and λ_2 are the wavelengths of consecutive peaks. The calculated SiO_2 film thickness is equal to 900 nm. This is a rough estimation because SiO_2 film refractive index is not constant through the spectral range of the measurements. It can expect that SHI-irradiation should change the refractive index value, too. Though, the calculated SiO_2 thickness is correlated with the SiO_2 film thickness measured by ellipsometry (1 μm). To prove our assumption of the interference effect, the reflectance spectrum was also registered (Fig. 3). The similar oscillation trend and coincidence of maxima in PL and reflectance spectra confirm the light interference after multiply reflections within the film. Taking the interference effect into account, one can suppose that the true PL of the samples irradiated with high fluencies (1×10^{14} and 5×10^{14} cm^{-2}) could be depicted as one white broad band centered at 550 nm. Annealing does not result in a noticeable PL spectrum change of the virgin sample and of the sample irradiated at 1×10^{10} cm^{-2}. On the contrary, PL quenching after annealing has revealed for the samples irradiated to higher fluencies (1×10^{12}–5×10^{14} cm^{-2}). A weak band at 440 nm is only recorded for these samples (not shown).

A passage of SHI through the silica can be followed by the formation of light-emitting Si nanoclusters in the ion tracks due to SiO_2 disproportionation. Structural and optical properties of SiO_2/Si structures irradiated with 167 MeV Xe ions and with 700 MeV Bi ions in a fluence range of 10^{12}–10^{14} cm^{-2} have been studied in Refs [14,15], and an appearance of yellow-orange photoluminescence after irradiation has been reported. PL intensity increased with the ion fluence up to 10^{14} cm^{-2} in the case of Xe and saturated at 5×10^{12} cm^{-2} in the case of Bi. The electronic energy loss amounts to ≈14.5 keV/nm for 167 MeV-Xe ions. This value is higher in comparison with $S_e \approx$ 13.5 keV/nm for 132 MeV-Xe ions (in our experiment). Though, a difference in 1.0 keV/nm is unsubstantial. It allows us to compare our results with data from Refs. [14,15] obtained for a-SiO_2 irradiated with Xe ions. In Refs [14,15] SHI-induced PL was ascribed to the formation of Si-riched nanostructures inside the ion tracks. This suggestion has been proved by scattering at 480 cm^{-1} registered in RS spectra of the irradiated samples. Its feature is typical of atomic vibrations in the amorphous Si.

For our samples, on the contrary to these results, RS method did not reveal any signs of the formation of amorphous or nanocrystalline Si phase in the SiO_2 samples neither after irradiation nor after annealing (not shown). The intensive peak at 520 cm^{-1} belonging to the crystalline Si wafer dominated in all RS spectra. We did not register the amorphous Si band at 480 cm^{-1} in irradiated samples. Commonly, the furnace annealing with a high thermal budget is applied [29–31] for the crystallization of amorphous nanoclusters and for a nanocluster's size increase. One could expect in our case that long-time annealing at 1100 °C should stimulate the crystallization of Si nanoclusters created in the ion tracks due to SiO_2 disproportionation (if any!). A presence of silicon nanocrystals should result in an appearance of low-energy tail of the Si-band at 520 cm^{-1} in RS spectra [32,33]. Though, we did not observe any Si-band shape distortion in RS spectra of irradiated and annealed SiO_2/Si structures.

The next step to reveal the formation of Si inclusions in SiO_2 was XTEM investigation of the irradiated samples. XTEM revealed no any structural transformation or precipitation in as-irradiated SiO_2 films. XTEM images of irradiated SiO_2 films after annealing were without any structural peculiarities, too (not shown). Hence, TEM results correlate with RS data and prove a conclusion of the Si nanoprecipitates absence in the irradiated SiO_2 films.

Thus, we can conclude that PL of the SiO_2 layers irradiated with swift Xe ions is not related with the Si nanoclusters formation. The other possible explanation of visible emission is a defect generation in the SiO_2 matrix by SHI irradiation. At first, let us discuss the luminescence of as-deposited SiO_2 and SiO_2 irradiated to the lowest fluence (1×10^{10} cm^{-2}). The PL spectrum of virgin SiO_2/Si sample includes only one weak band at 450 nm. A similar PL band was observed for the pure SiO_2 in Ref. [34] and attributed to F_2 colour centre. An existence of such colour centres is due to the formation of oxygen deficient defects. The irradiation with Xe ions to the fluence of 1×10^{10} cm^{-2} does not results in any noticeable PL spectrum transformation. As it is mentioned above the latent tracks are the regions of high concentration of oxygen deficient defects. Though, track overlapping for the fluence of 1×10^{10} cm^{-2} is negligible. Correspondingly, a part of irradiated SiO_2 matrix occupied with the latent tracks is negligible, too, and a damage level of SiO_2 matrix, at whole, remains low enough. Annealing does not alter the PL spectra of the virgin sample and the sample irradiated to the lowest fluence. Taking this into account, we attribute the band at 450 nm to native defects in silicon dioxide.

A weak green band at 550 nm in the PL spectrum of the sample irradiated to the fluence of 1×10^{12} cm^{-2} can be ascribed to F_4 oxygen deficient center [34]. Obviously, the oxygen deficient defect concentration increases with fluence, and the formation of more complicated radiative centers such as F_4 takes place in the irradiated layer. As it was shown above, the true PL of the samples irradiated to the higher fluencies ($\geq 10^{14}$ cm^{-2}) could be depicted as one white broad band centered at 550 nm. The similar white band was observed in the PL spectra of a-SiO_2 irradiated with 5 MeV Kr ions to fluencies of (10^{15} -10^{16}) cm^{-2} [34]. This PL band was attributed to the formation of radiative oxygen deficient centers. Under condition of multiple tracks overlapping, we can suggest the formation of a variety of oxygen deficient defect complexes in irradiated SiO_2. Apparently, these features are responsible for white PL of the irradiated a-SiO_2 observed in our experiment.

Fig. 4 depicts the PL peak intensity as a fluence function. One can

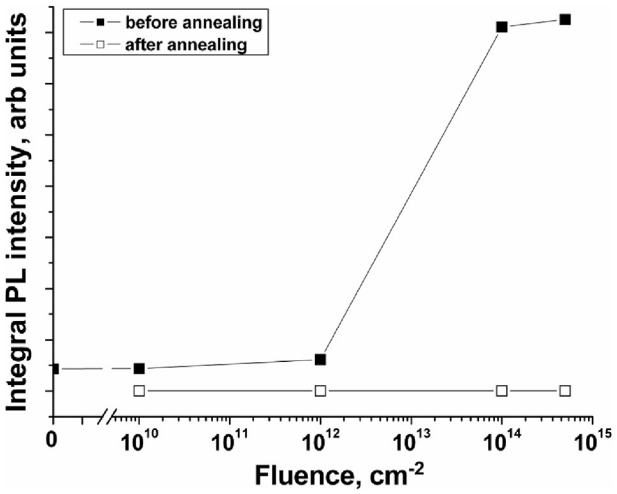

Fig. 4. The integral PL intensity of SiO_2 films irradiated at different fluencies: (-■-) as-irradiated samples, (–□–) irradiated samples after annealing at 1100 °C for 2 h (the lines are there to guide the eyes). The PL intensity of virgin sample is marked as a point at the vertical axis.

see that in the range of low fluencies (10^{10} - 10^{12}) cm^{-2} the PL signal intensity is weak and practically the same as one from the non-irradiated sample. The PL signal increases by 10 times with the fluence increase from 10^{12} to 10^{14} cm^{-2} and saturates at 5×10^{14} cm^{-2}. The authors of Ref. [15] reported "the PL peak intensity-fluence" dependence for a-SiO_2 films irradiated with 167 MeV Xe ions in a fluence range of 10^{12}–10^{14} cm^{-2}. One can see from Ref. [15] that PL intensity of irradiated samples is practically the same at the Xe ion fluencies of 10^{12} and 3×10^{12} cm^{-2}. Further the PL signal intensity increases continuously with fluence up to 10^{14} cm^{-2}. It is correlated with our results. Though, because we covered the more extended fluence range, the PL signal saturation at 5×10^{14} cm^{-2} was observed.

It is interesting to compare the fluence dependencies of PL intensity and etch velocity (Figs 2 and 4). In general, both PL intensity and etch velocity increases with ion fluence. However, despite similarity between results some differences are observed, too. Unlike of the PL intensity, the etch velocity is continuously increases with fluence up to 5×10^{14} cm^{-2}, more slowly at low fluencies and more quickly in the fluence range of (1×10^{14}–5×10^{14}) cm^{-2}. One would expect a saturation of the etching velocity at these high fluences because multiple overlapping of individual damaged zones. But, it is not happened. It is known that the differences in the etch velocity are induced by the deformation fields around damaged zones (see, for example [35]). Obviously, the process of mechanical stress accumulation lasts yet at the fluence higher than 10^{14} cm^{-2} resulting in the modified etching rate. The similar feature of fluence dependencies is practically full recovery of both PL intensity and etch velocity to the initial values after high-temperature treatment.

It is known that the long-time heat treatment results in the decomposition of defect's complexes or their conversion to non-radiative recombination centers. That is why we did not register a noticeable visible luminescence from the high-fluence irradiated samples after annealing at 1100 °C. Tyschenko [36] reported the similar results on the visible PL of a-SiO_2 films implanted with 200 and 100 keV-Si ions to fluencies of 3×10^{16} and 1.8×10^{16} cm^{-2}, respectively. SiO_2 films were annealed at (400–1000 °C) for 30 min after the irradiation. On the base of analysis of the PL dependence on annealing temperature, the author of Ref [36] concluded that the implantation-induced PL of SiO_2 was due to radiative oxygen deficient centers and noticed that the heat-treatment of implanted SiO_2 at 1000 °C resulted in visible PL quenching. These results are in a good agreement with our results.

As it was mentioned above, a rearrangement of six-component rings consisting of SiO_4-tetrahedra into three- and four-component rings takes place along the latent SHI track in a-SiO_2 resulting in the emergence of microscopic defects with stressed Si–O bonds in the form of paramagnetic E′ centers and oxygen deficient defects [16,25–27]. Heat-treatment is accompanied by a damage recovery in the irradiated SiO_2 film, and the reconstruction of six-component rings from small rings induced by SHIs irradiation takes place again. It should result in the V_{irr} recovery to the initial value as we observe in our experiment. It should be mentioned that Awazu et al. [16] have studied the structure of latent tracks created in amorphous SiO_2 using the IR absorption spectroscopy and chemical etching in HF. They reported the complete etch rate recovery to the initial value after annealing the irradiated samples at 600 °C for 150 min in inert ambient.

4. Conclusions

We have studied the etch velocity in 4% - HF and the visible PL of 1 μm-thick SiO_2 films thermally grown on Si and afterwards irradiated with 133 MeV Xe ions to the fluencies ranging between 10^{10} cm^{-2} and 5×10^{14} cm^{-2}.

It was found a drastic increase of the SiO_2 etch velocity in HF solution at the fluence of $\geq 10^{14}$ cm^{-2}. The etch velocity ratio of irradiated and virgin SiO_2 (V_{irr}/V_{virgin}) amounts to 2.2 and 4.1 for the fluence of 1×10^{14} cm^{-2} and 5×10^{14} cm^{-2}, respectively. Annealing of irradiated samples (1100 °C, 120 min) resulted in a restoration of the etch velocity practically to its virgin value. The V_{irr}/V_{virgin} ratio can be useful in order to estimate the radiation damage in a-SiO_2 matrix irradiated with high fluencies of SHIs.

An intensive visible luminescence was registered from the samples irradiated to the fluence of 10^{14} cm^{-2} and higher. The PL signal intensity was saturated at the fluence of 5×10^{14} cm^{-2}. Kachurin et al. [14,15] consider Si inclusions to be responsible for visible luminescence of SHI-irradiated a-SiO_2. Presumably, such inclusions can be formed via SiO_2 disproportionation in the ion tracks. In our experiment, TEM and RS data did not prove the formation of Si nanoprecipitates in the as-irradiated a-SiO_2 as well as in the irradiated a-SiO_2 after heat treatment. We believe that an appearance of visible PL is due to the generation of oxygen deficient defects and its complexes in the SiO_2 matrix irradiated with SHIs in conditions of multiple ion track overlapping. The PL signal quenching after annealing of irradiated samples (1100 °C, 120 min) supports additionally a suggestion of SHIs-induced defect's responsibility for a-SiO_2 visible luminescence.

References

[1] D.A. Young, Nature 182 (1958) 375–377.
[2] M. Toulemonde, C. Dufour, A. Meftah, E. Paumier, Nucl. Instr. Meth. B166–167 (2000) 903–912.
[3] M. Toulemonde, G. Li, V. Shuttanandan, P. Kluth, T. Yang, Y. Wang, Y. Zhang, Phys. Rev. B 83 (2011) 054106 (9 pp).
[4] L.A. Vlasukova, F.F. Komarov, V.N. Yuvchenko, W. Wesch, E. Wendler, A.Yu Didyk, V.A. Skuratov, S.B. Kislitsin, Vacuum 105 (2014) 107–110.
[5] L. Vlasukova, F. Komarov, V. Yuvchenko, L. Baran, O. Milchanin, A. Dauletbekova, A. Alzhanova, A. Akilbekov, Vacuum 129 (2016) 137–141.
[6] A. Dallanora, D.A. Marcondes, T.L. Bermudez, G.G. Fichtner, C. Trautmann, M. Toulemonde, R.M. Papaleo, J. Appl. Phys. 104 (2008) 024307 (8 pp).
[7] F. Bergamini, M. Bianconi, S. Cristiani, L. Gallerani, A. Nubile, S. Petrini, S. Sugliani, Nucl. Instr. Meth. B266 (2008) 2475–2480.
[8] L.A. Vlasukova, F.F. Komarov, V.N. Yuvchenko, O.V. Mil'chanin, A.Yu Didyk, V.A. Skuratov, S.B. Kislitsyn, Bulletin of the Russian academy of sciences, Physics 76 (2012) 582–587.
[9] E. Yu Kaniukov, J. Ustarroz, D.V. Yakimchuk, M. Petrova, H. Terryn, V. Sivakov, A.V. Petrov, Nanotechnology 27 (2016) 115305 (13pp).
[10] C. D'Orleans, J.P. Stoquert, C. Estourne's, C. Cerruti, J.J. Grob, J.L. Guille, F. Haas, D. Muller, M. Richard-Plouet, Phys. Rev. B 67 (2003) 220101. R (4 pp).
[11] F. Singh, S. Mohapatra, J.P. Stoquert, D.K. Avasthi, J.C. Pivin, Nucl. Instr. Meth. B 267 (2009) 936–940.
[12] D.K. Avasthi, Y.K. Mishra, F. Singh, J.P. Stoquert, Nucl. Instr. Meth. B 268 (2010) 3027–3034.
[13] F.F. Komarov, O.V. Milchanin, V.A. Skuratov, M.A. Makhavikou, A. Janse van Vuuren, J.N. Neethling, E. Wendler, L.A. Vlasukova, I.N. Parkhomenko, V.N. Yuvchenko, Bulletin of the Russian academy of sciences, Physics 80 (2016) 141–145.
[14] G.A. Kachurin, S.G. Cherkova, D.V. Marin, V.G. Kesler, V.A. Volodin, V.A. Skuratov, Nucl. Instr. Meth. B 282 (2012) 68–72.
[15] S.G. Cherkova, G.A. Kachurin, V.A. Volodin, A.G. Cherkov, D.V. Marin, V.A. Skuratov, Optoelectronics, Instrum. Data Proseccing 50 (2014) 93–100.
[16] K. Awazu, S. Ishii, K. Shima, S. Roorda, J.I. Brebner, Phys. Rev. B 62 (2000) 3689–3698.
[17] http://www.srim.org.
[18] Gmelin Handbook of Inorganic and Organometallic Chemistry. Si. Suppl. Vol. B5e. eighth ed.. Springer-Verlag. 1994. P. 264.
[19] A. Benyagoub, M. Toulemonde, J. Mat. Res. 30 (2015) 1529–1543.
[20] P. Kluth, C.S. Schnohr, O.H. Pakarinen, F. Djurabekova, D.J. Sprouster, R. Giulian, M.C. Ridgway, A.P. Byrne, C. Trautmann, D.J. Cookson, K. Nordlund, M. Toulemonde, Phys. Rev. Lett. 101 (2008) 175503 (4 pp).
[21] B. Canut, M.G. Blanchin, S. Ramos-Canut, V. Teodorescu, M. Toulemonde, Nucl. Instr. Meth. B 245 (2006) 327–331.
[22] F.F. Komarov, L.A. Vlasukova, P.V. Kuchinskyi, A. Yu Didyk, V.A. Skuratov, N.A. Voronova, Lithuanian J. Phys. 49 (2009) 111–115.
[23] S.K. Shrivastava, K. Ganesan, P. Gangopadhyay, B.K. Panigrahi, K.G.M. Nair, A.K. Tyagi, Nucl. Instr. Meth. B 338 (2014) 89–94.
[24] P. Kluth, O.H. Pakarinen, F. Djurabekova, R. Giulian, M.C. Ridgway, A.P. Byrne, K. Nordlund, J. Appl. Phys. 110 (2011) 123520 (5 pp).

[25] R.A.B. Devine, Nucl. Instr. Meth. B91 (1994) 378–390.
[26] M.C. Busch, S. Slaoui, P. Siffert, E. Dooryhee, M. Toulemonde, J. Appl. Phys. 71 (1992) 2596–2601.
[27] K. Awazu, H. Kawazoe, J. Appl. Phys. 94 (2003) 6243–6262.
[28] P. Mazzoldi, A. Carnera, F. Caccavale, M.L. Favaro, A. Boscolo-Boscoletto, G. Granozzi, R. Bertoncello, G. Battaglin, J. Appl. Phys. 70 (1991) 3528–3536.
[29] M. Molinari, H. Rinnert, M. Vergnat, J. Appl. Phys. 101 (2007) 123532 (8 pp).
[30] G. Scardera, T. Puzzer, G. Conibeer, M.A. Green, J. Appl. Phys. 104 (2008) 104310 (7 pp).
[31] Z.H. Cen, T.P. Chen, L. Ding, Y. Liu, J.I. Wong, M. Yang, Z. Liu, W.P. Goh, F.R. Zhu, S. Fung, J. Appl. Phys. 105 (2009) 123101 (6 pp).
[32] D. Nesheva, C. Raptis, A. Perakis, I. Bineva, Z. Aneva, Z. Levi, S. Alexandrova, H. Hofmeister, J. Appl. Phys. 92 (2002) 4678–4683.
[33] F. Komarov, L. Vlasukova, I. Parkhomenko, O. Milchanin, A. Mudryi, A. Togambaeva, O. Korolik, Thin Solid Films 579 (2015) 110–115.
[34] S. Yin, Z. Chong-hong, M. Yan-cheng, Z. Heng-qing, Z. Li-qing, G. Jie, Y. Yi-tao, M. Yi-zhun, Nucl. Instr. Meth. B 326 (2014) 68–71.
[35] F. Komarov, V. Uglov, L. Vlasukova, A. Didyk, S. Zlotski, V. Yuvchenko, Nucl. Instr. Meth. B360 (2015) 150–155.
[36] I.E. Tyschenko, Semiconductors 49 (2015) 1176–1180.